Electronic Supplementary Material (ESI) for Soft Matter.

Supporting Information

Table S1. Molecular weight and polydispersity index of polymer samples.

Polymers	Lot #	M_w	PDI
P3BT	BS19-36	41k	2.3
P3OT	PTL11-39	63k	1.9
P3DT	PTL11-77	57k	2.1
P3DDT	BS21-87	39k	1.8
PQT-12	DL158	40k	1.7
PBTTT-C12	16C0103	20k	1.55
Regiorandom P3HT	BS20-92	63k	2.4

1. Electrode Polarization

In order to exclude the electrode polarization effect due to ions in the solvents, the following experiments were performed. If ions contribute to the measurement, the origins of ions may come from either the solvents or from impurities in the dissolved polymers. To test this while preventing the formation of nanofibers, regiorandom P3HT was used since it will not crystallize into nanofibers due to its random side chain configuration. Consequently, two sets of samples were prepared: solvent mixtures of dodecane and 1,2-dichlorobenzene and the same samples containing 30 mg/ml regiorandom P3HT. The configuration was identical to the parallel plates geometry described on page 9 of the main text. Moreover, if any of the above samples induce electrode polarization, changes in permittivity should be observed as a function of electrode separation distance. Therefore, both sets of samples were measured at 0.5mm and 0.25 mm distances to compare the results.

From the result in Figure S1 below, solvent and regiorandom P3HT samples are almost identical to each other at all of the different gap distances. Moreover, the value of ε' is much lower than that found for electric field aligned P3HT fibers. Therefore, the high permittivity at low frequency should be attributed to the assembled P3HT structure. Impedance spectroscopy measurement carried out by other groups on solid P3HT films, also show a uptake of permittivity at low frequency. [1–3]

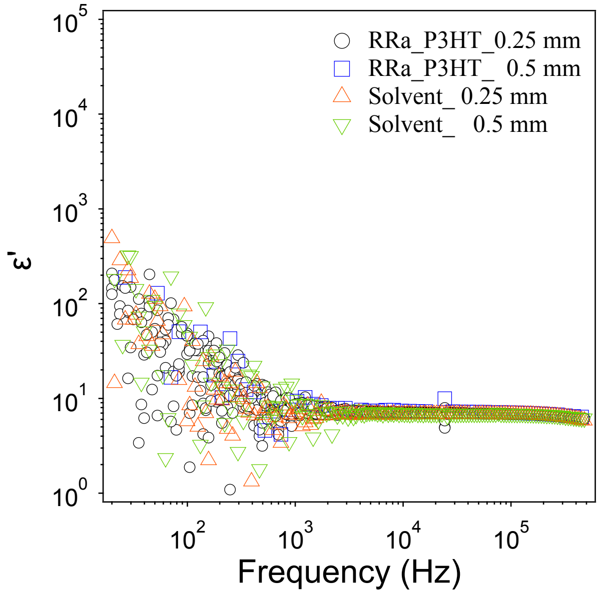

Figure S1. Permittivity of 30 mg/ml regiorandom P3HT in 25 wt% dodecane and 75 wt% 1,2-dichlorobenzene mixture and its solvent as a function of frequency. Both samples were conducted at two different gap distances: 0.25 and 0.5 mm, respectively. The experiment was performed in the same way as the dielectric spectroscopy measurement described in the main text. The voltage amplitudes used were 20 mV.

2. FFT Transform

FFT transformation of model images was also used in order to better understand the meaning of features that were observed. Figure S2 shows FFTs performed on artificially generated images that were treated identically to the experimental images. Clearly, horizontal alignment results in the formation of vertical features of high intensity in the FFT. Interestingly, when lines are spaced with a repeating distance (Figure S2a), the intensity concentrates in two high intensity ‘points’ similar to a diffraction pattern. When randomness is introduced in the separation distance, the ‘points’ diffuse and lead to a high intensity ‘stripe’. In FFT from experimental images, we observe features that are characteristic of both of these cases.

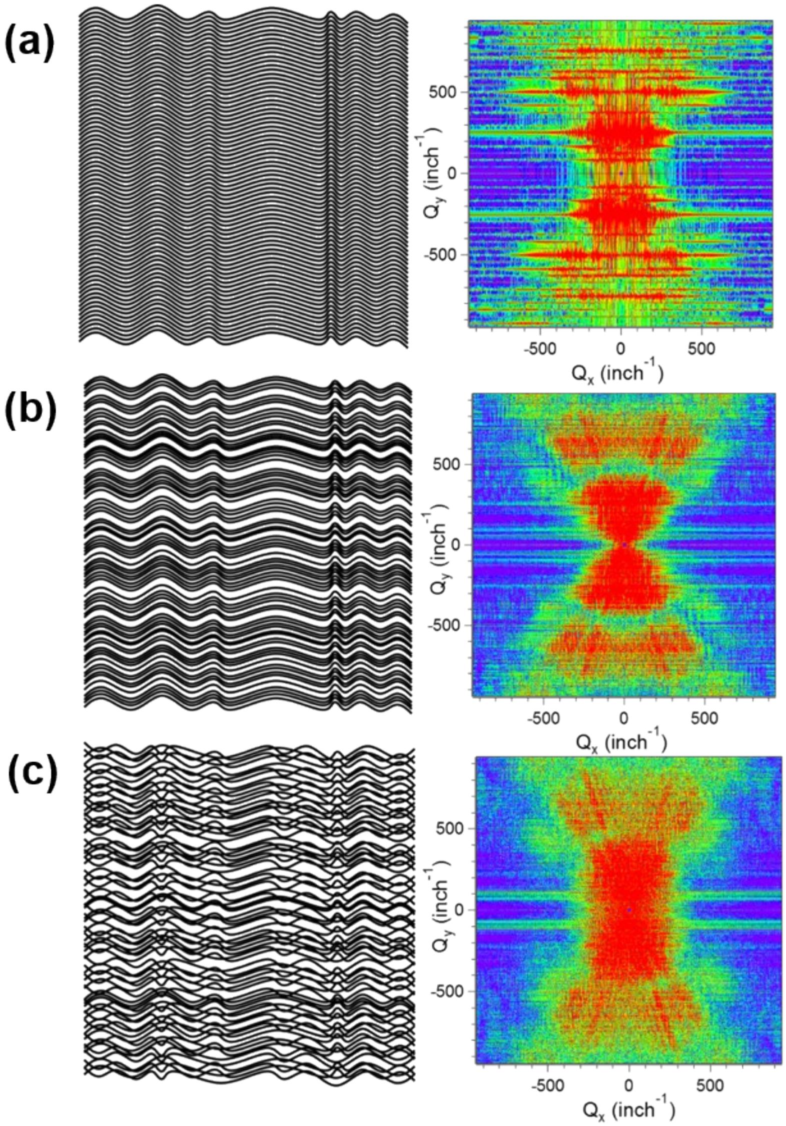

Figure S2. Raw images of artificially generated lines and corresponding FFT transform of (a) equally spaced (b) randomly spaced and (c) entangled fibers. Two dots appear in the FFT image if the fibers are well aligned and with equal distance as in (a). In contrast, the loss of alignment in (c) shows a vertical stripe for entangled fibers.

3. Concentration Dependence of Alignment

The effect of changing crystallization kinetics was also investigated by varying P3HT concentrations as is shown in Figure S3. Although fiber alignment was observed at all concentrations, the degree of order varied significantly. In FFT images, the vertical lines at higher concentrations shifted towards lower k_y values, which corresponded to increased size and broader distribution. It is interesting to note that the optimum electric field condition would not change with increasing concentrations. Experiments performed with variable frequency and amplitude using a more concentrated sample (30 mg/ml P3HT) resulted the same optimum conditions as for 1 mg/ml P3HT. The optical microscopic images and the corresponding FFT images of the electric field sweep of 30 mg/ml P3HT are shown in Figure S4 ~ S6.

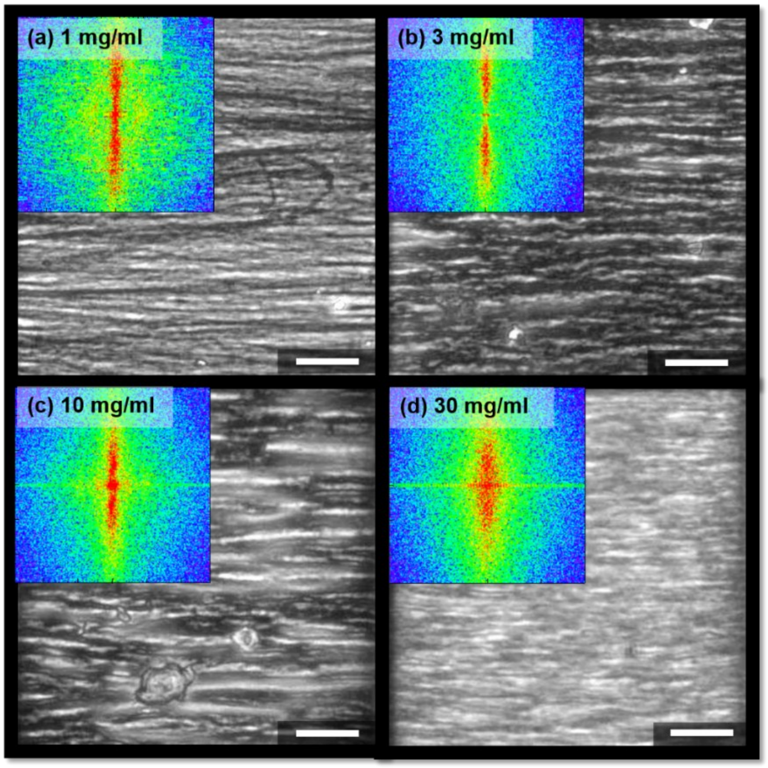

Figure S3. Microscopic images of P3HT fibers aligned under 160V/mm 250Hz in 25% wt dodecane mixed with dichlorobenzene at concentrations of (a) 1 (b) 3 (c) 10 (d) 30 mg/ml. The insets showed the corresponding FFT of each concentration. The scale bars represent 20 µm.

4. Electric Field Dependence: Frequency and Amplitude (30 mg/ml)

Experiments with variable frequency and amplitude were also performed using samples with larger

P3HT concentration. Figure S4 and S5 demonstrate that an optimum condition for alignment is also observed for these samples. Annular integrations were summarized in Figure S6 for different electric field conditions. Interestingly, these conditions seem to be very close to the optimum frequency (250 Hz) and amplitude (160 V/mm) that were observed at the lower P3HT concentrations (1 mg/mL) that are shown in Figure 2a,b. However, it is important to note that the quality of the aligment was significantly higher when lower concentrations of polymer were being used. It is very likely that this is also due to the difficulties that arrise when trying to image the thicker and more opaque samples that result when using the higher concentrations of P3HT.

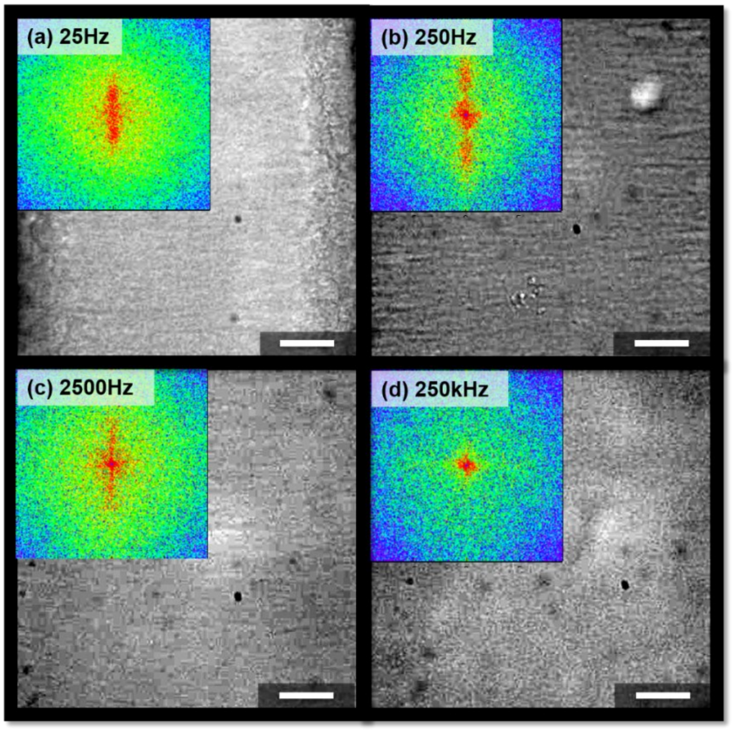

Figure S4. Microscopic images of 30mg/ml P3HT in 25% dodecane balanced with 75 wt% 1,2-dichlorobenzene under 160V/mm and (a) 25 (b) 250 (c) 2500 (d) 250000 Hz electric fields. The insets showed the corresponding FFT images and the scale bars represent 20 μm.

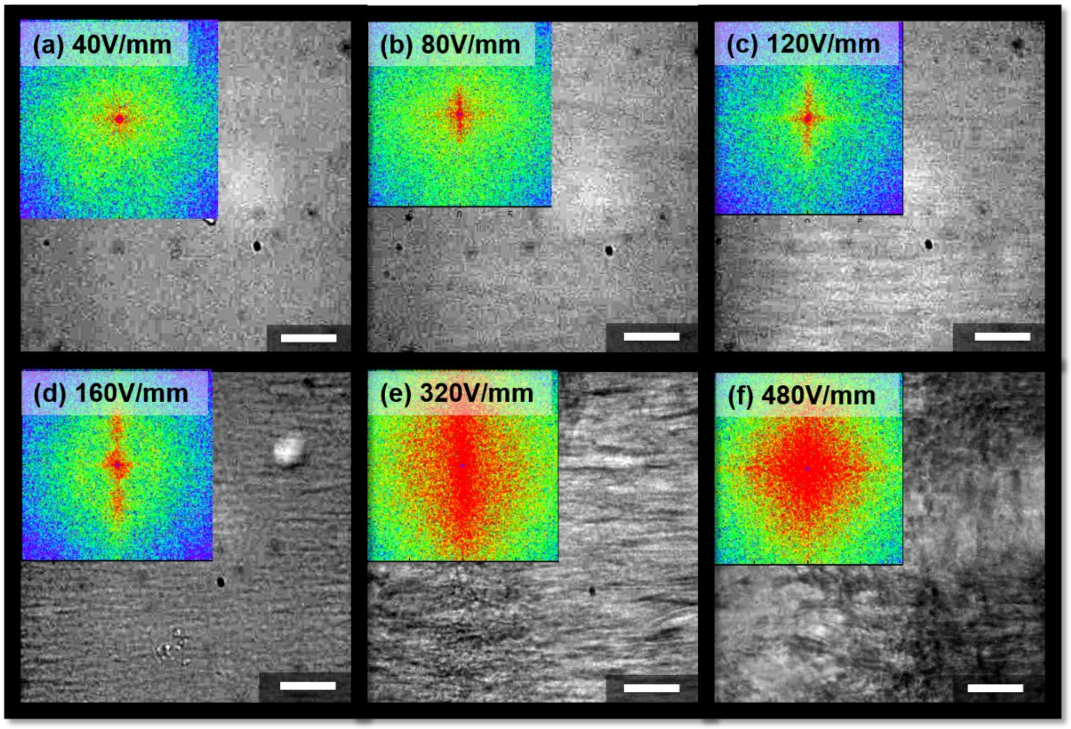

Figure S5. Microscopic images of 30 mg/ml P3HT in 25% wt dodecane mixed with 75 wt% 1,2-dichlorobenzene under 250Hz and (a)40 (b) 80 (c) 120 (d) 160 (e) 320 (f) 480 V/mm electric fields applied between two silver electrodes with 125μm gap. The insets show the FFT of the optical imgaes and the scale bars represent 20 μm.

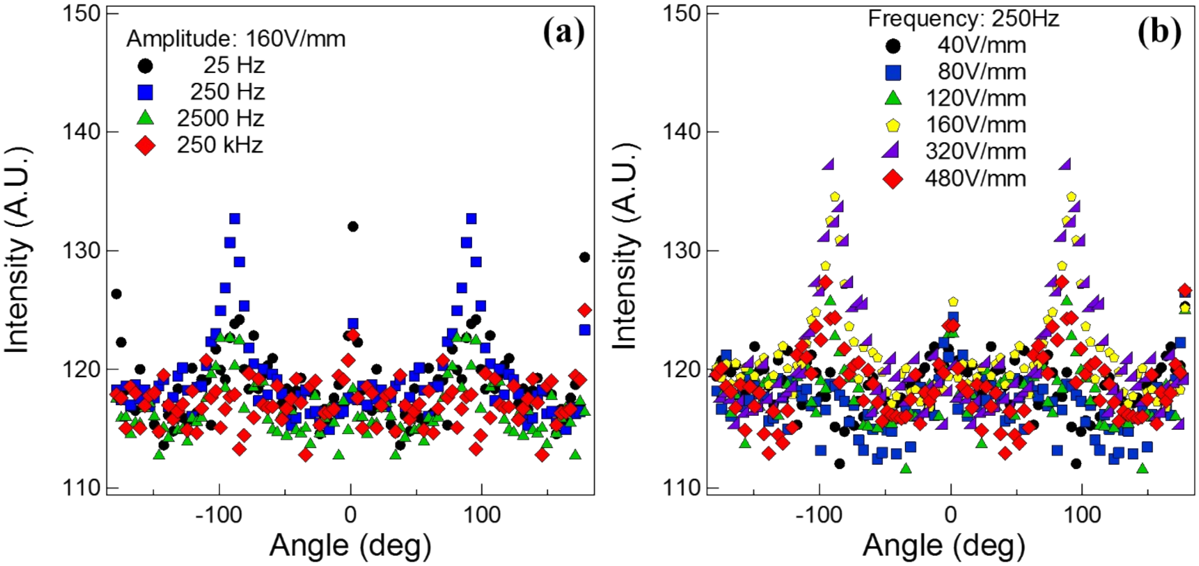

Figure S6. Annular integrations of the 2-D FFT images in Figure S4 and S5 of electric fields (a) fixed amplitude with varying frequencies and (b) constant frequency with changing amplitudes.

5. Influence of Solvent Quality on Electric Field Alignment

Dodecane is a poor solvent for P3HT so that a higher fraction in the solvent results in higher supersaturation and faster nucleation and growth for the fibers.[4–6] Figure S7 shows the results of experiments performed for a series of samples (30 mg/mL P3HT) having different dodecane ratios under identical electric field conditions (250 Hz and 200 V/mm). In pure dichlorobenzene solutions, Figure S7(a), P3HT remained fully dissolved and no self-assembly occurred before the evaporation of the solvent. As a result, FFT images are homogeneous and no alignment or fiber formation is visible. When the dodecane content was increased, the formation of aligned fibers was observable and reached a maximum alignment at a dodecane fraction of 25 wt%. In contrast, when the dodecane ratio was increased to 40 wt%, the supersaturation was very high and the kinetics of crystallization was too fast to allow for organized alignment to occur. An elastic organogel formed quickly and fibers interconnected before the DEP force was able to transport them along the electric field gradient.

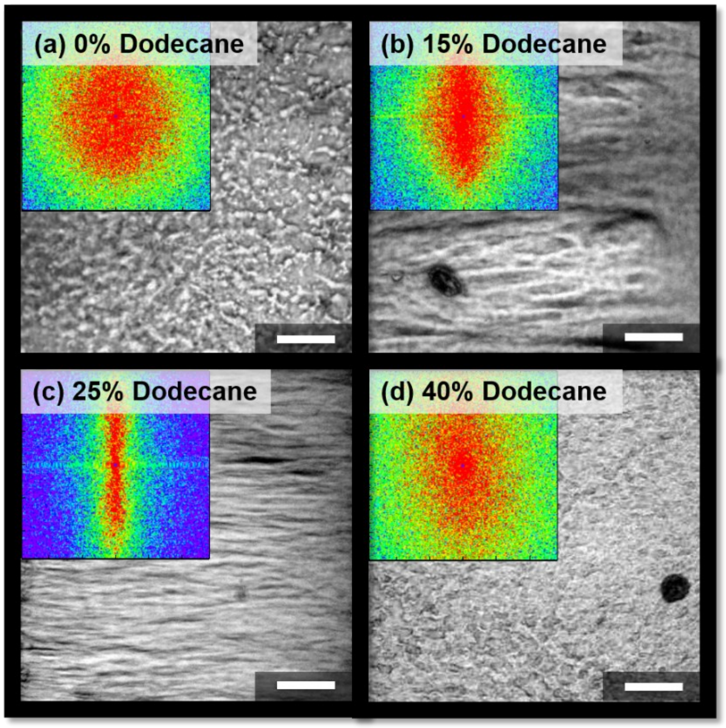

Figure S7. Microscopic images of P3HT fibers after gelation in mixed solvents of (a) 0% (b) 15% (c) 25% and (d) 40%wt dodecane balanced with dichlorobenzene under 250Hz 200V/mm electric field. The insets are the corresponding FFT images and the scale bars represent 20 µm.

6. Atomic Force Microscopy

AFM images were recorded *via* Bruker Dimension Icon-PT atomic force microscope with peak force tapping mode. A scan of a 10 µm × 10 µm area was used. Samples for AFM were prepared by drop casting P3HT dissolved in 35 wt% dodecane and 65 wt% 1,2-dichlorobenzene solution over substrates with embedded parallel electrodes. To produce the AFM image in Figure 1 (main manuscript), a Si wafer was used having a 200 nm thermally grown SiO_2 layer and patterned layers of chromium (12 nm) and gold (50 nm) in a parallel electrode system with a 100 μm gap. Gold and cadmium layers were patterned by a standard photolithography process. The frequency sweep experiments in Figure S8 and Figure S9 were conducted using P3HT samples coated over glass microscope slides with silver electrodes separated by 125 μm. The electric fields were applied for 20 min, followed by a hexane wash to remove the high boiling point solvents. The samples were dried in air overnight before taking AFM images.

Figure S8 shows the atomic force microscopic images of 1 mg/ml P3HT aligned at variable frequencies. In Figure S8 (a) to (c) it is clear that the micron size fibers, which consist of bundled nanofibers, are aligned unidirectionally and formed at lower frequencies (i.e. 25 Hz and 250 Hz). The height of the fiber bundles formed at 25 Hz is higher than that of 250 Hz on the surface. At higher frequencies (i.e. 2.5-250 kHz) corresponding to Figure S8 (d) to (f), the long-range order deteriorates gradually and the fiber heights are reduced. To rule out the possibility that this loss of order at high frequencies was due to the formation of very thick samples, samples at much lower P3HT concentrations (0.1 mg/ml) were also prepared and analyzed with AFM. These results are shown in Figure S9. A dependence of alignment on frequency was also found for these samples and no alignment was observed above 2.5 kHz.

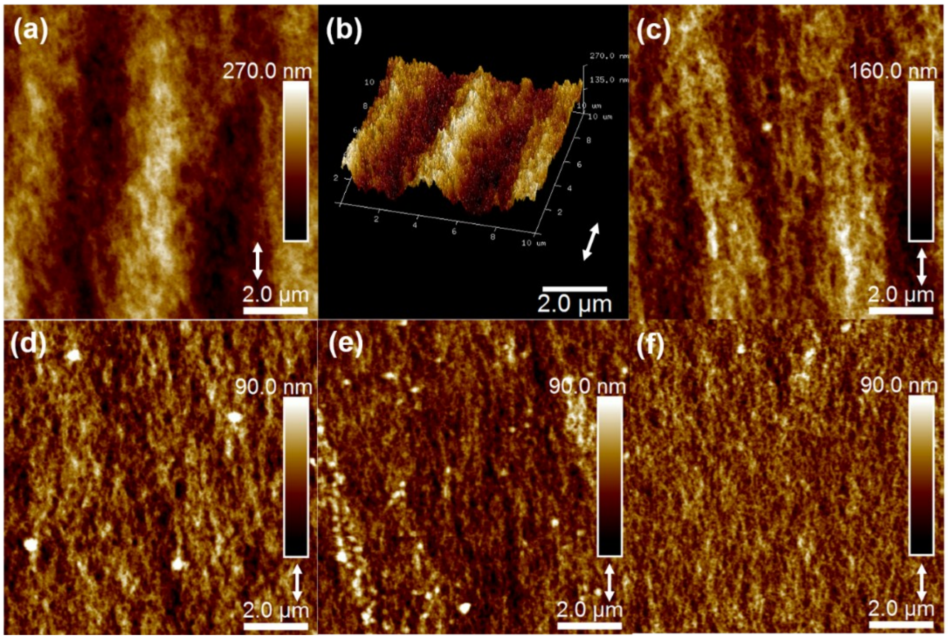

Figure S8. AFM images of 1 mg/ml P3HT in 25 wt% dodecane and 75 wt% 1,2-dichlorobenzene aligned under 160V/mm and (a) 25 Hz, (c) 250 Hz, (d) 2.5 kHz, (e) 25 kHz, and (f) 250 kHz electric field. Figure 5(b) is the 3-D view of Figure 5(a). The arrow at the bottom right corner of each image represents the direction of the electric field.

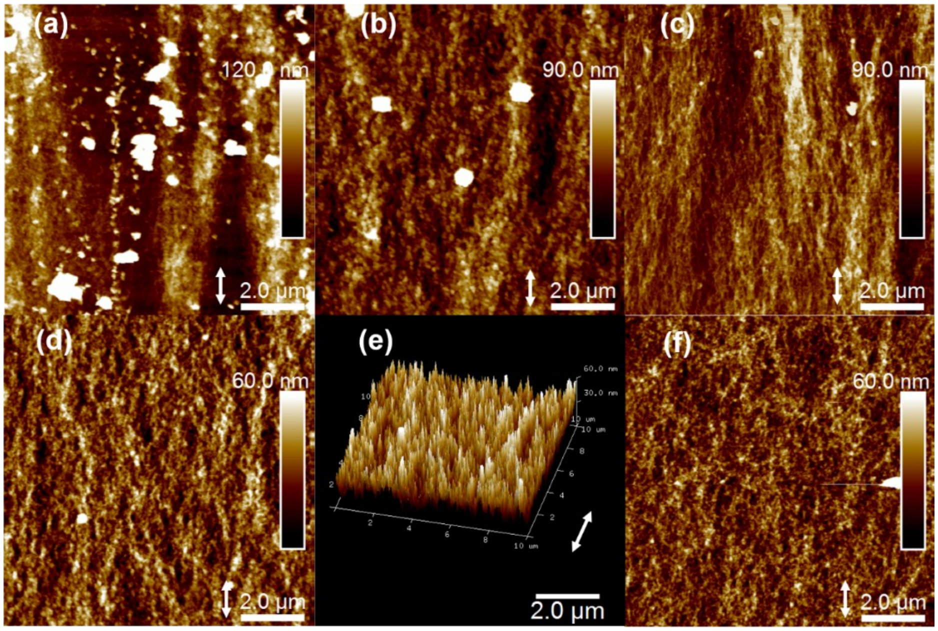

Figure S9. AFM images of 0.1 mg/ml P3HT in 25 wt% dodecane and 75 wt% 1,2-dichlorobenzene aligned under 160V/mm and (a) 25 Hz, (b) 250 Hz, (c) 2.5 kHz, (d) 25 kHz, and (f) 250 kHz electric field. (e) is the 3-D view of (d). The arrows at the bottom right corner indicate the direction of electric fields.

7. SANS Fitting

In order to extract more quantitative information from SANS experiments, direct 2-D fitting was performed using an aligned cylinder model at two electric field conditions that resulted in alignment: 200 V/mm and 400 V/mm at 250Hz. The SANS results and the corresponding fits are shown in Figure S10. The fitting was performed by keeping three parameters as variables: cylinder radius (r), length (l), and standard deviation of tilt angle θ with respect to the electric field direction (i.e. horizontal). An explanation is shown in Figure S11 (a). In perfectly aligned samples without deviations, the value of θ is 0°. During fitting, the mean value of the distribution was fixed at 0°and the standard deviation of the distribution was fit. The fit results are shown in a table in figure S11 (b). It is noteworthy that higher electric field amplitudes resulted in fibers with smaller standard deviation of θ. This is consistent with our proposed mechanism that higher amplitude resulted in larger DEP force, which can transport smaller fibers and improve orientation along the electric field direction. The angular distribution is also plotted in Figure S11 (c)

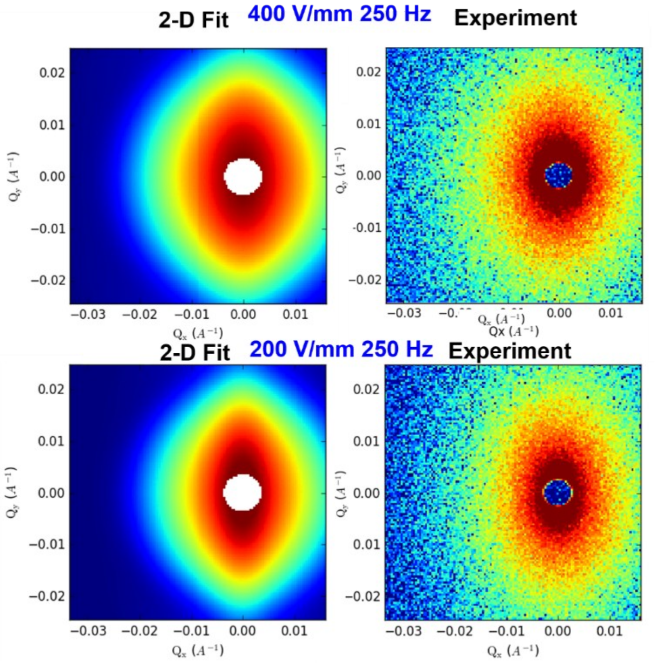

Figure S10. 2-D fitting of the SANS data based on cylinder model for 200V/mm at 250Hz and

400 V/mm at 250Hz electric field alignment conditions, respectively.

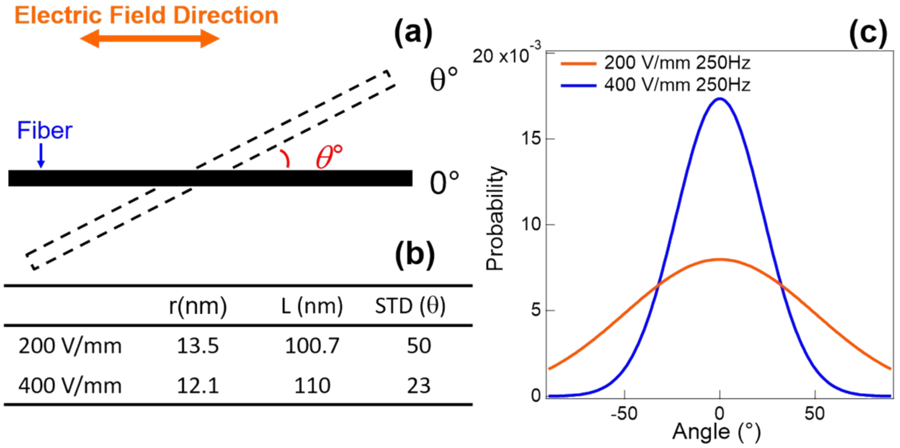

	r(nm)	L (nm)	STD (θ)
200 V/mm	13.5	100.7	50
400 V/mm	12.1	110	23

Figure S11. (a) Schematic of a perfectly aligned fiber (θ = 0°) and a fiber with a finite angle θ relative to horizontal direction. (b) Cylinder radius (r), cylinder length (l) and standard deviation of θ (mean was fixed at θ = 0°) obtained from 2-D fitting. (c) Angular distributions from 2D SANS fits for 200 and 400 V/mm.

8. Rheology

The repeatability of the rheology measurement in Figure 5 is plotted in semi-log scale and shown in Figure S12. It is clear that the application of the AC field strengthens the gel while the application of DC fields results in a weaker gel.

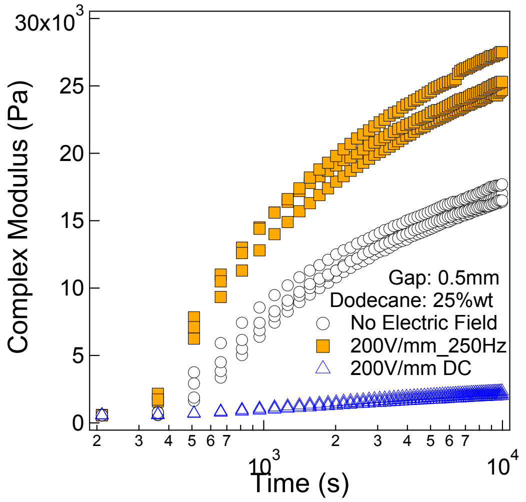

Figure S12. Complex modulus for 30 mg/ml P3HT samples in 25 wt% dodecane mixed with DCB formed with 0, 200 V/mm 250Hz and 200 V/mm DC electric fields as a function of time. Three samples were repeated and shown for each conditions.

9. Fractal Dimensions obtained from rheology and SANS

Linear fit of rheology kinetics based on Liu's model and power law fit of the SANS data at low q range to extrapolate fractal dimensions.

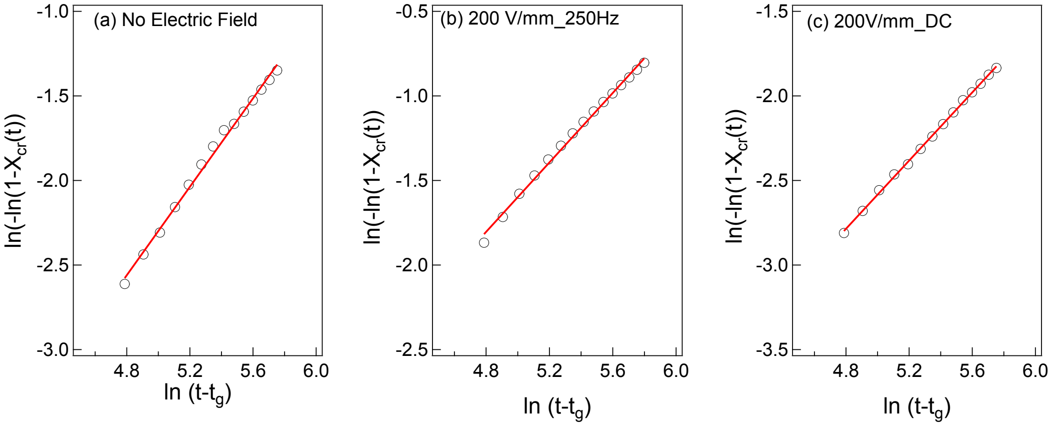

Figure S13. Plots of ln(-ln(1-X_{cr}(t)) as a function of ln(t-tg) based on rheological properties G* according to Liu's model for (a) without, (b) with 200 V/mm 250Hz and (c) 200 V/mm DC electric field aligned samples, whereas $X_{cr}(t) = \frac{G^*(t) - G^*_0}{G^*(max) - G^*_0}$. The open circles are the experimental data and the solid red lines are the corresponding fits.

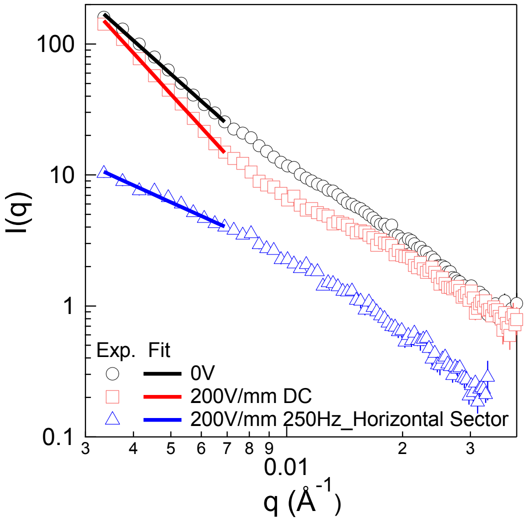

Figure S14. Reduced 1-D profile of SANS data using customized sample cell depicted in Figure 3 with neutron beam perpendicular to the electric field. The 2-D pattern at 200V/mm 250Hz electric field is reduced by sector integration along horizontal direction. For 0V and 200V/mm DC samples, the 1-D profile is obtained by circular integration. The regions from 0.0033 to 0.007 Å^{-1} are fitted with power law to obtain the fractal dimension (D_f^S).

10. Dielectric Spectroscopy and FEM Analysis

Dielectric loss, imaginary and real part of conductivity obtained from dielectric spectroscopy measurement are shown in Figure S15 as supplement of dielectric permittivity in Figure 6 (b).

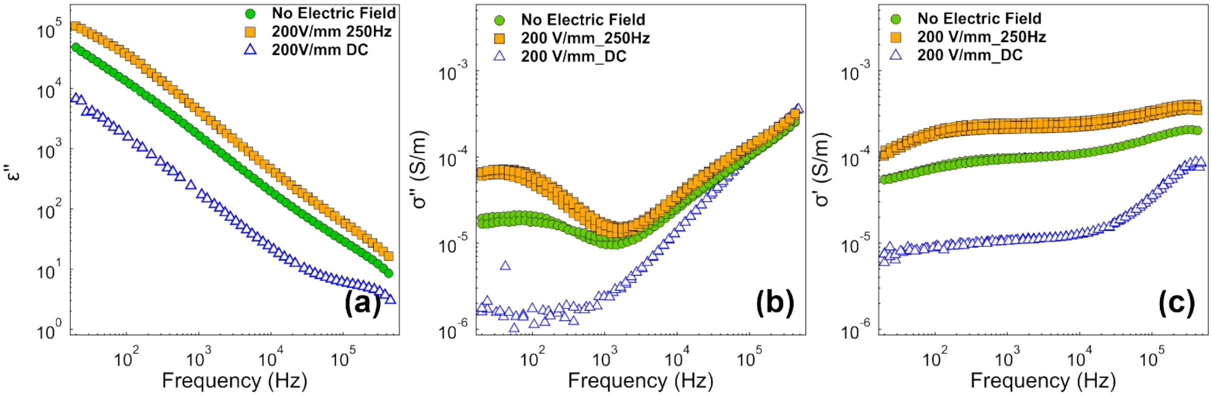

Figure S15. (a) Dielectric loss, (b) imaginary and (c) real part of conductivity as a function of frequency. The data was obtained from the dielectric spectroscopy of P3HT organogel in Figure 9 in the main text.

The simulation of electric field gradient distribution between two electrodes was conducted *via* COMSOL Multiphysics software. The electrostatics physics module was used and all of the simulations were performed in 2-D domains. The profiles corresponding to the parallel-plate electrodes were directly imported from an experimental profilometer roughness measurement. The Maxwell's Equation was used as the governing equation. The system was meshed with free triangular shape of element sizes between 6 nm and 3 μm. Charge conservation and electrode potentials were used as boundary conditions. Continuity relation was applied for the transition between adjacent materials.

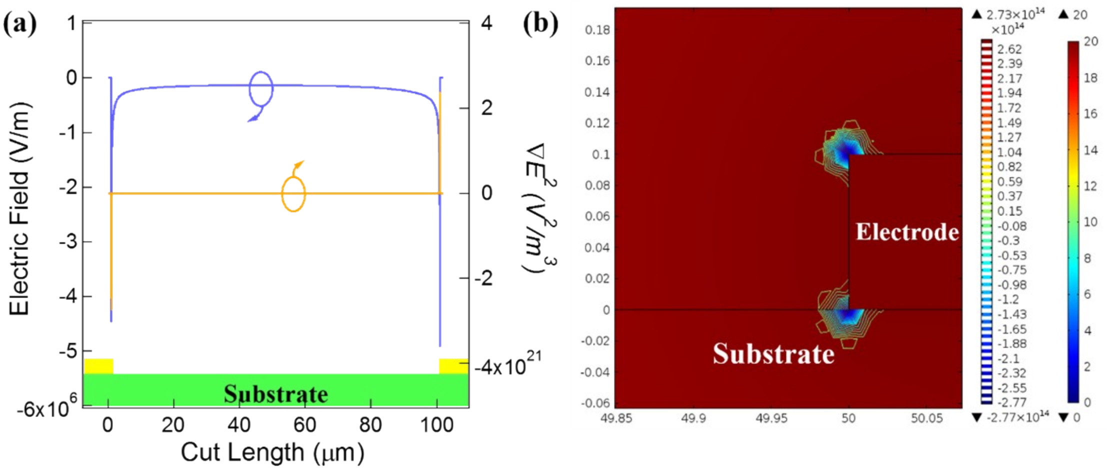

Figure S16. (a) Simulations of electric field and gradient of electric field squared distributions between two planar electrodes with a 100 μm gap under 20V electrical potential. (b) 2-D potential distribution and electric field contours simulated by COMSOL.

In both SANS and rheology measurements, the electrodes applying electric fields were parallel plates with a ~1 mm separation distance. Although two perfectly flat parallel plates lead to ideally uniform electric field gradient, local electric field gradients, serving to nucleate initial fibers, can be induced by roughness of the electrodes. A Bruker OM-Dektak XT Profilometer was used to measure the roughness of the Ti plates that were used for SANS measurements. The scan length was 3mm and three different positions were measured on the plates and averaged to extract a representative roughness value. The root mean square roughness of the titanium plates used for SANS measurement was 3.92 ± 0.23 μm. The electric field for a rough plate was also simulated by FEM and the gradient of electric field squared, ∇E^2, was plotted in Figure S17. The overall magnitude of ∇E^2 dropped by about six orders of magnitude when compared to that of the planar electrodes used in microscopy as shown in Figure S16. Still, the DEP force would still be large enough to transport the nanofibers when they grow to be large. It is also important to note that the roughness of the electrodes only determines the electric field gradient at initial stages. The electric field would be significantly distorted as soon as some nanofibers start to grow and this further accelerates assembly.

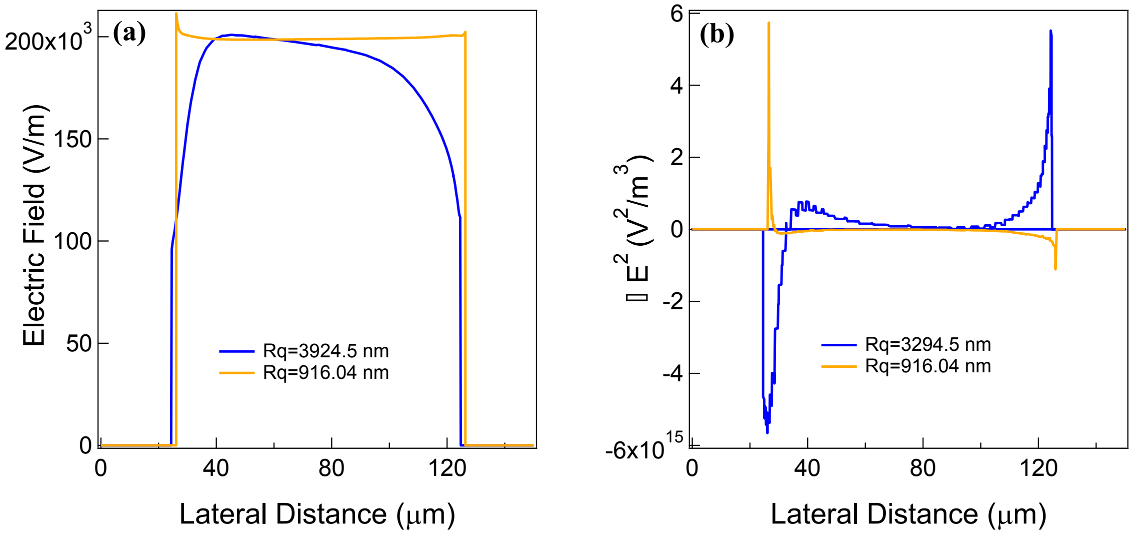

Figure S17. (a) Simulations of electric field distribution between two parallel plates with different roughness separated by 100 μm under 20V electric potential. (b) Simulations of the gradient of electric field squared between two parallel plates with different roughness separated by 100 μm under 20V electric potential. The roughness was measured with profilometer and the profile was used as the edge of the electrodes. The magnitude of the gradient of electric field squared dropped by six order of magnitudes compared to planar geometry in Figure S16 (a).

12. Dielectrophoretic Force Calculations

The real part of Clausius-Mossotti function, which is shown in Figure S18 (a), was used to calculate DEP force in Figure 8 (main text). According to Equation-6 in the main text, this factor determines the signs of torque at x, y, and z directions. These are plotted in Figure S 18 (b) as a function of frequency.

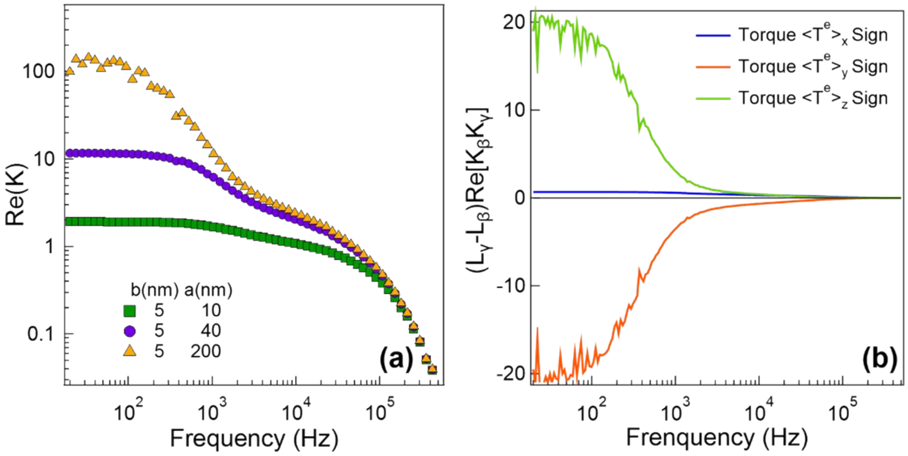

Figure S18. (a) Comparison of the real part of Clausius-Mossotti function for fully dissolved P3HT coil and nanofibers with different sizes. Radius of gyration is used to describe the size of fully dissolved polymer chains. “a” represents the length and “b” denotes the radius of the nanofibers. (b) Factor $(L_\gamma\text{-}L_\beta)\mathrm{Re}[\underline{K}_\beta\underline{K}_\gamma]$ as a function of frequency determines the sign of the torques for different axis. The blackline indicates “0” torque, which separates positive and negative signs.

13. Zeta Potential

Zeta potential measurements were performed on a Zetasizer Nano HT from Malvern Instruments (Worchestershire, U.K.) using a 1 cm path length quartz dip cell with 633 nm wavelength laser. The P3HT samples were made in 0.3 mg/ml concentrations in 45 wt% dodecane mixed with 55 wt% dichlorobenzene and diluted by 40 times for the measurements. The samples were prepared in ambient air or in an argon filled glovebox. A sphere shape was assumed and the Huckel electrokinetic model was used in calculating zeta potential values.

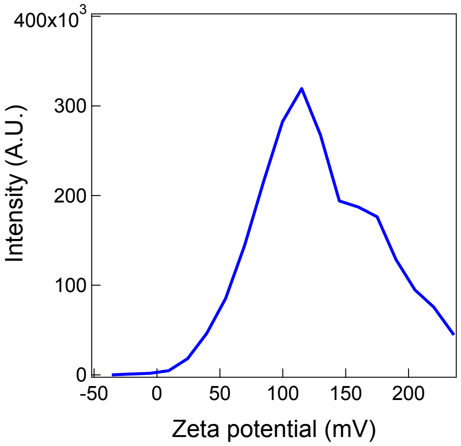

Figure S19. Zeta potential measurement of 1 mg/ml P3HT colloidal network prepared in 25 wt% dodecane mixed with 75 wt% dichlorobenzene.

14. Time Resolved SANS

Time-resolved SANS data are shown in Figure S20 with and without electric fields. The slope of the low-q region (0.0037 to 0.007 Å^{-1}) showed a slight decrease from the beginning to the end of the gelation process. The exponent (slope in log-log plot) at the early stage indicates the presence of some large scale heterogeneous structures. Since these aggregates are large, they scatter with a large exponent due to Porod scattering (i.e. q^{-4}). A combined model of large spheres (i.e. aggregates) and dissolved polymer was used to fit the scattering profile at early stages in Figure S20 (c) (300s) and to estimate the amount of aggregation that would lead to this low-q increase. The fit estimated that a very small amount of aggregates (i.e. 0.65% of the total vol% of polymer) with 63 nm in radius was enough to reproduce scattering profile. As the sample crystallizes and nanofibers form, the scattering is rapidly dominated by these emerging nanostructures and the exponent at low-q is reduced. The origin of the aggregates could be contaminants in polymer samples, such as insoluble polymer or residual catalyst. Another possible cause of the low-q signal is due to the error in correcting empty cell scattering, since the rough electrodes also have large features (>1 μm) that can contribute to low-q scattering. Great efforts have been made to correct for it by increasing empty cell counting time and by measuring every empty cell for each corresponding sample, but the excess signal was not fully eliminated. However, it is important to note that the initial large aggregates at low-q region do not affect the cross-sectional dimensions extrapolated from parallelpiped model, which is performed at mid and high-q region (0.01 ~ 0.3 $Å^{-1}$) in Figure S20.

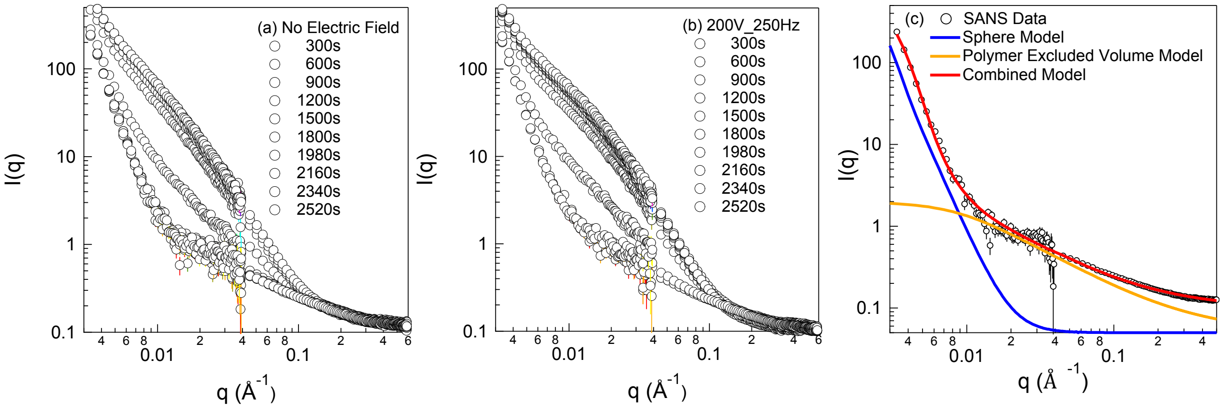

Figure S20. SANS of gelation process (a) without and (b) with electric field as a function of time with 30 mg/ml P3HT in 25 wt% dodecane and 75 wt% 1,2-dichlorobenzene in the dielectric cell that has been reported before.[7,8] (c) SANS data of 30 mg/ml P3HT in a mixed solution of 25 wt% dodecane and 75 wt% 1,2-dichlorobenzene collected at 300s and the corresponding fitting using combined model of sphere and polymer excluded volume model.

15. UV-Vis Spectroscopy

A Thermo Evolution 300 UV-Vis spectrophotometer was used to record the absorption spectra at wavelength between 300 and 800 nm. 30 mg/ml P3HT samples dissolved in 25% wt dodecane mixed with 1,2-dichlorobenzene was loaded between two parallel plates and experiment performed in the same way as the rheology measurement described in the main context. After allowing gelation for 3 hrs, a small amount of sample was taken out to disperse at a concentration below 0.1 mg/ml in the same solvent used to prepare the gel. Redissolved samples were prepared by heating up the dispersed fibers to ~80 °C to fully dissolve them. Filtrate curves were obtained by filtering dispersed samples with 200 nm pore size syringe filters (VWR, Radnor, PA). Concentration were determined using Beer's law by fitting the peak absorbance at ~450 nm of the fully dissolved P3HT to extract extinction coefficient.

UV-Vis spectroscopy was also utilized to indirectly probe for structural changes caused by the electric fields. UV-Vis spectra are shown in figure S21 where the solid fraction of fibers were also calculated and compared. The method used for calculating fiber fractions, which was similar to that used in previous publications, consist of filtration and separation of the dissolved fraction.[9] The main absorbance peak in the dissolved state ($\lambda \sim 450$ nm) for a fully dissolved sample ($A_{\text{redissolved}}$) and for the extracted supernatant after filtration (A_{filtered}) were used to calculate the fiber/solid fraction using equation 1. The absorption spectra for crystalline, re-dissolved, and filtered samples are all shown in Figure S21. A small increase of the solid fraction from 79.3% to 84.7% was observed after applying an electric field. According to Clark and coworkers,[10] the ratio of the 0-0 and 0-1 peak absorbance can be used to calculate the free exciton bandwidth (W). Values of W for samples formed with and without electric field were 31.2 and 47.1 meV, respectively. Lower W values suggest a higher order for the interchain π-π stacking. Thus, samples without electric field showed relatively higher order of the π-π stacking than those with electric field.

$$\phi_s = 1 - \frac{A_{filtered}}{A_{redissolved}} \qquad \text{Eq-1}$$

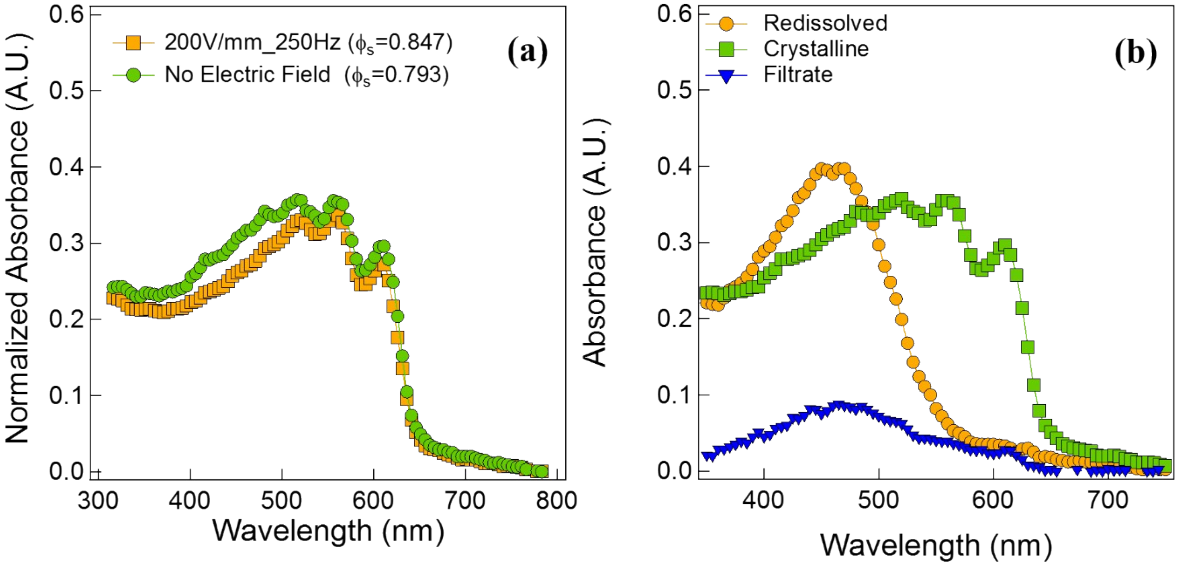

Figure S21. (a) Absorption spectra for a fraction of 30 mg/ml P3HT samples formed in rheology measurement with 200 V/mm 250Hz and without electric field alignment at room temperature. (b) Absorption spectrum for P3HT that was redissolved at 80 ºC, crystalized in solution, as well as the supernatant of the solution with solid P3HT removed by filtration.

16. Model Fitting of SANS Data

Time-resolved SANS data taken at 2520 s is fitted with parallelpiped and polymer excluded volume combined model. The fitting is plotted with SANS data in Figure S22 with the cross-sectional dimensions labeled in the inset. The size of the electric field aligned sample (200 V/mm 250 Hz) is similar to that without electric fields.

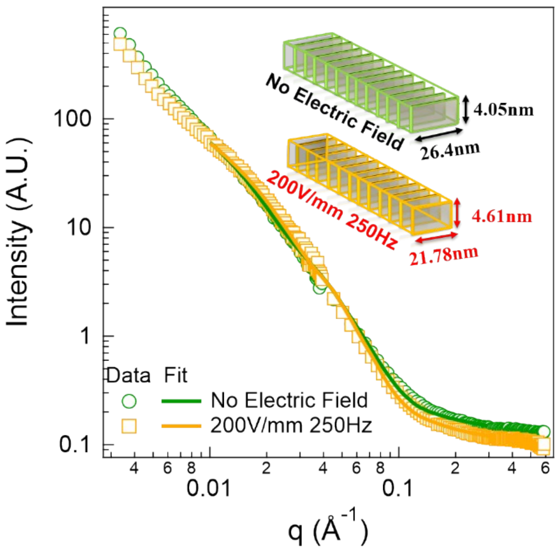

Figure S22. Combined model fitting of the scattering profiles at 2520s. The inset picture showed the dimensions of the cross-section from the fitting.

17. Conjugated Polymer Alignment

Conjugated polymers with similar structure to P3HT can be aligned in electric fields. P3DDT and regio-random P3HT were the only polymers that could not be aligned. Images of alignment are shown in Figure S23.

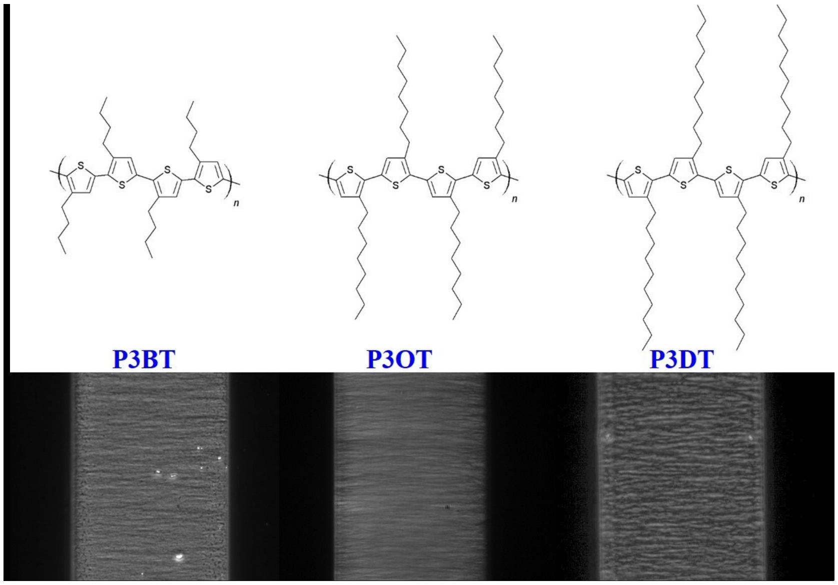

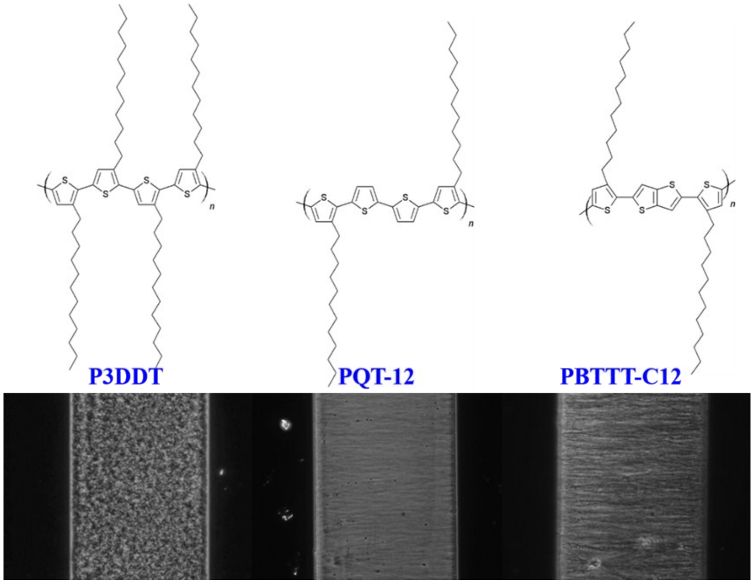

Figure S23. Molecular structure and the corresponding electric field alignment using 160 V/mm and 250 Hz of P3BT, P3OT, P3DT, P3DDT, PQT-12 and PBTTT-C12 dissolved in 25 wt% dodecane balanced with 75 wt% 1,2-dichlorobenzene.

References:

1 J. Obrzut and K. A. Page, *Phys. Rev. B*, 2009, **80**, 195211.

2 R. Singh, R. K. Singh, J. Kumar, R. Kant and V. Kumar, 2010, **48**, 1047–1053.

3 M. Okutan, S. E. San, Z. Alpaslan and A. Demir, 2011, **2011**.

4 J.-L. Li, B. Yuan, X.-Y. Liu and H.-Y. Xu, *Cryst. Growth Des.*, 2002, **10**, 2699–2706.

5 P. D. La Iglesia and D. C. Pozzo, *Soft Matter*, 2013, **9**, 11214.

6 X. Y. Liu, P. D. Sawant, W. B. Tan, I. B. M. Noor, C. Pramesti and B. H. Chen, *J. Am. Chem. Soc.*, 2002, **124**, 15055–15063.

7 G. M. Newbloom, K. M. Weigandt and D. C. Pozzo, *Soft Matter*, 2012, **8**, 8854.

8 G. M. Newbloom, K. M. Weigandt and D. C. Pozzo, *Macromolecules*, 2012, **45**, 3452–3462.

9 G. M. Newbloom, F. S. Kim, S. a. Jenekhe and D. C. Pozzo, *Macromolecules*, 2011, **44**, 3801–3809.

10 J. Clark, J. F. Chang, F. C. Spano, R. H. Friend and C. Silva, *Appl. Phys. Lett.*, 2009, **94**, 2007–2010.